Ready Access to Anhydrous Anionic Lanthanide Acetates by Using Imidazolium Acetate Ionic Liquids as the Reaction Medium

Guillaume Bousrez,[a] Olivier Renier,[a] Steven P. Kelley,[b] Brando Adranno,[a] Elnaz Tahavori,[a] Hatem M. Titi,[c] Volodymyr Smetana,[a] Si-Fu Tang,[d] Anja-Verena Mudring,*[a] and Robin D. Rogers*[a, e]

Abstract: Access to lanthanide acetate coordination compounds is challenged by the tendency of lanthanides to coordinate water and the plethora of acetate coordination modes. A straightforward, reproducible synthetic procedure by treating lanthanide chloride hydrates with defined ratios of the ionic liquid (IL) 1-ethyl-3-methylimidazolium acetate ($[C_2mim][OAc]$) has been developed. This reaction pathway leads to two isostructural crystalline anhydrous coordination complexes, the polymeric $[C_2mim]_n[\{Ln_2(OAc)_7\}_n]$ and the dimeric $[C_2mim]_2[Ln_2(OAc)_8]$, based on the ion size and the ratio of IL used. A reaction with an IL:Ln-salt ratio of 5:1, where Ln = Nd, Sm, and Gd, led exclusively to the polymer, whilst for the heaviest lanthanides (Dy–Lu) the dimer was observed. Reaction with Eu and Tb resulted in a mixture of both polymeric and dimeric forms. When the amount of IL and/or the size of the cation was increased, the reaction led to only the dimeric compound for all the lanthanide series. Crystallographic analyses of the resulting salts revealed three different types of metal-acetate coordination modes where $\eta^2\mu\kappa^2$ is the most represented in both structure types.

Introduction

The simple acetate anion ($[OAc]^-$) is ubiquitous in Nature and offers an exciting coordination chemistry because of the plethora of coordination modes it can accommodate with metal ions (Figure 1, right), especially in anionic metal complexes.[1] With larger metal ions such as alkaline earths (Ae^{2+}), lanthanides (Ln^{3+}), or uranyl ($[UO_2]^{2+}$), structurally distinct anionic complexes form structures ranging from isolated monomers chelated by $[OAc]^-$, to dinuclear oligomers and polymeric complexes with chelating, bridging, and mixed coordination modes.[2] Some Ln^{3+} ions, for example, Nd^{3+}, have been found with up to three different metal/ligand ratios, pointing towards the large hidden potential of these systems to provide unique acetate complexes.[2] This wide range of coordination modes which $[OAc]^-$ can adopt with the lanthanides prompted us to explore reproducible routes to homoleptic anionic salts of the series of 4*f* elements. Only a few structures of homoleptic 4*f*-element acetate complexes have been reported so far.[3] A particular challenge in the preparation of homoleptic complexes of trivalent lanthanides is their extreme oxophilicity, ubiquitous water frequently enters their coordination environment.

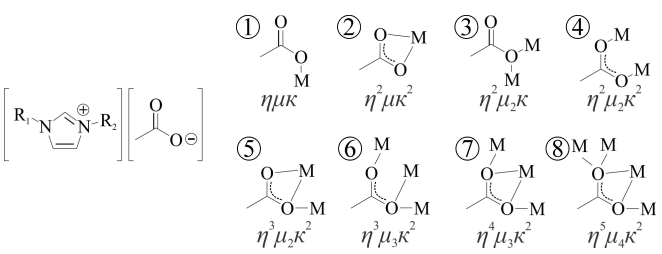

Figure 1. Top: General structure of dialkylimidazolium acetate ILs. Bottom: Observed coordination modes of the $[OAc]^-$ ion with trivalent lanthanide cations.

[a] Dr. G. Bousrez, O. Renier, B. Adranno, E. Tahavori, Dr. V. Smetana, Prof. A.-V. Mudring, Prof. Dr. R. D. Rogers
Department of Materials and Environmental Chemistry
Stockholm University
Svante Arrhenius väg 16 C, Stockholm 10691 (Sweden)
E-mail: anja-verena.mudring@mmk.su.se

[b] Dr. S. P. Kelley
Department of Chemistry, University of Missouri
601, S. College Avenue, Columbia, MO 65211 (USA)

[c] H. M. Titi
Department of Chemistry, McGill University
Montreal, QC H3A 0B8 (Canada)

[d] Prof. Dr. S.-F. Tang
College of Chemistry and Pharmaceutical Sciences
Qingdao Agricultural University
Changcheng Road 700, Chengyang District
Qingdao 266109 (P. R. China)

[e] Prof. Dr. R. D. Rogers
College of Arts & Sciences
The University of Alabama
Tuscaloosa, AL 35401 (USA)
E-mail: rdrogers@ua.edu

Supporting information for this article is available on the WWW under https://doi.org/10.1002/chem.202100141

As a vehicle to provide a high concentration of coordinating ligands promoting the formation of homoleptic complexes, and large stable cations (e.g., dialkylimidazolium cations, Figure 1, left) which can stabilize large and potentially unusual coordination complex anions, ionic liquids (ILs) have proven a valuable synthetic tool, in particular for obtaining homoleptic complexes.[2,4] Their tendency to promote coordination of large numbers of anions and the exclusion of neutral solvent molecules has led to new coordination numbers, various coordination modes, and polymeric structures,[5] in addition to providing routes to new luminescent and magnetic materials.[6]

One feature of ILs, which renders them particularly interesting as solvents and reaction media for the conversion of hydrates, particularly for the readily hydrated lanthanide salts, is the stability of ILs to temperatures above the boiling point of water. Certain ILs with coordinating and even weakly coordinating anions[7] can be reacted neat with hydrated metal salts on the benchtop and heated, with or without vacuum, to drive off volatiles such as such as H_2O or even HCl.[8] Historically, access to anhydrous lanthanide complexes has been limited because of their high affinity for oxygen,[9] thus we have been exploring the use of ILs to dehydrate metallic salts leading to ready access to new compounds including $[C_2mim][UO_2(OAc)_3]$, $[C_2C_2im][UO_2(OAc)_3]$, $[C_4mim][UO_2(OAc)_3]$, $[C_2C_2im]_2[La(OAc)_5]$, $[C_2mim]_2[Nd(OAc)_5]$, and $[C_2mim]_n[Sr(OAc)_3]_n$ (where (C_2mim) = 1-ethyl-3-methylimidazolium, (C_2C_2im) = 1,3-diethylimidazolium, (C_4mim) = 1-butyl-3-methyl-imidazolium).[2,4a,8] Interestingly, in these reactions the formation of oxo- and hydroxy compounds, which frequently occurs when attempting to dehydrate hydrates of strongly Lewis basic metal salts, is suppressed. Moreover, while readily accessible coordination chemistry is thus easily available, systematic studies are still lacking.

In this work, we build upon our observation that the readily available IL $[C_2mim][OAc]$ allows for easy and reliable access to water-free *f*-element compounds and develop a general, reliable synthetic procedure applicable across the entire range of 4*f* metal ions leading to anhydrous materials. Here, single crystal X-ray diffraction analysis has allowed us to unveil the complex nature of acetate coordination modes in these anhydrous, homoleptic lanthanide anionic complexes across the entire lanthanide series.

Results and Discussion

Synthesis

The synthetic methodology developed (Scheme 1) is based on reacting readily available starting salts such as $LnCl_3 \cdot xH_2O$ (Ln = La, Pr, Nd, Sm–Lu, x = 6 or 7) with an excess of the IL $[C_2mim][OAc]$ in a fixed molar ratio, driving off the water by heating, and slowly cooling to obtain a crystalline product. The crystalline complexes were characterized by powder and single crystal X-ray diffraction (PXRD and SCXRD), differential scanning calorimetry (DSC), and infrared spectroscopy (IR).

When using a 5:1 IL:Ln-salt molar ratio, a combination of PXRD and SCXRD revealed the formation of two series of

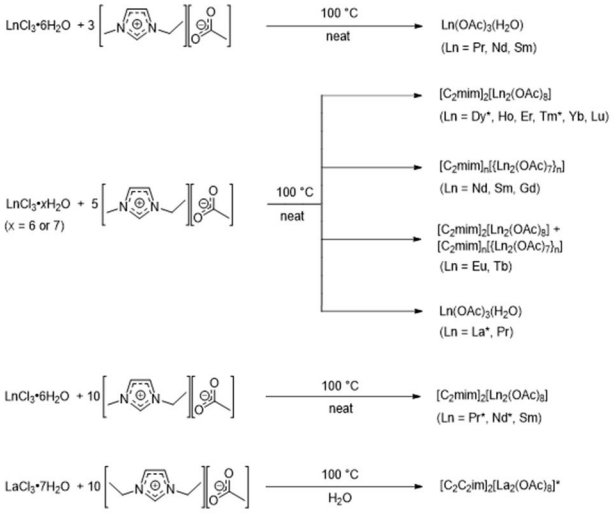

Scheme 1. General scheme of the synthesis of anhydrous salts of anionic 4*f*/$[OAc]^-$ complexes and influence of the amount of IL introduced on the selectivity of the final product. (*: PXRD indicates that these compounds were obtained, albeit along with unidentified side products.)

anhydrous, homoleptic lanthanide acetate complexes, dimeric $[C_2mim]_2[Ln_2(OAc)_8]$ (Ln = Eu, Tb–Lu) and polymeric $[C_2mim]_n[\{Ln_2(OAc)_7\}_n]$ (Ln = Nd, Sm–Tb). For the largest lanthanides tested, La and Pr, only $Ln(OAc)_3(H_2O)$ could be isolated (Figure S4 in the Supporting Information). A detailed description of their structures can be found below. Whilst this reaction with light lanthanides (Nd, Sm, and Gd) led to the formation of exclusively polymeric $[C_2mim]_n[\{Ln_2(OAc)_7\}_n]$ (see Figure S1 for PXRD patterns of the products), with the heaviest lanthanides (Dy–Lu) the formation of dimeric $[C_2mim]_2[Ln_2(OAc)_8]$ was observed (see Figure S2 for PXRD patterns of the products). The reaction with the intermediate lanthanides, Eu and Tb, resulted in a mixture of both polymeric and dimeric forms (PXRD patterns are shown in Figures S3, S5, and S6). The PXRD patterns of representatives for each of the two compound series, $[C_2mim]_n[\{Ln_2(OAc)_7\}_n]$ (Ln = Gd) and $[C_2mim]_2[Ln_2(OAc)_8]$) (Ln = Er) are shown in Figure 2. However, even if in most cases the final products are obtained as phase pure, for some lanthanides the PXRD patterns indicated that some minor unidentified side products were generated during the reaction.

There are multiple effects which could result in the preferential formation of each of the three compounds like the ion size or lanthanide salt concentration in the IL, that is, IL–Ln-salt ratio. To shed more light on this, several experiments were conducted.

To investigate whether it is truly the decreasing ion size, and/or the IL:Ln-salt ratio that leads to the preferential formation of $[C_2mim]_2[Ln_2(OAc)_8]$ (which would correspond to $[C_2mim][OAc] \cdot Ln(OAc)_3$) over $[C_2mim]_n[\{Ln_2(OAc)_7\}_n]$ (which could be re-written as $0.5[C_2mim][OAc] \cdot Ln(OAc)_3$) different IL:Ln-salt ratios, namely 3:1 and 5:1 molar equivalents (equiv.) were tested (Scheme 1).

When the reactions were conducted with 3 equiv. of IL, the large lanthanides (Pr, Nd, and Sm) yielded only $Ln(OAc)_3(H_2O)$ as

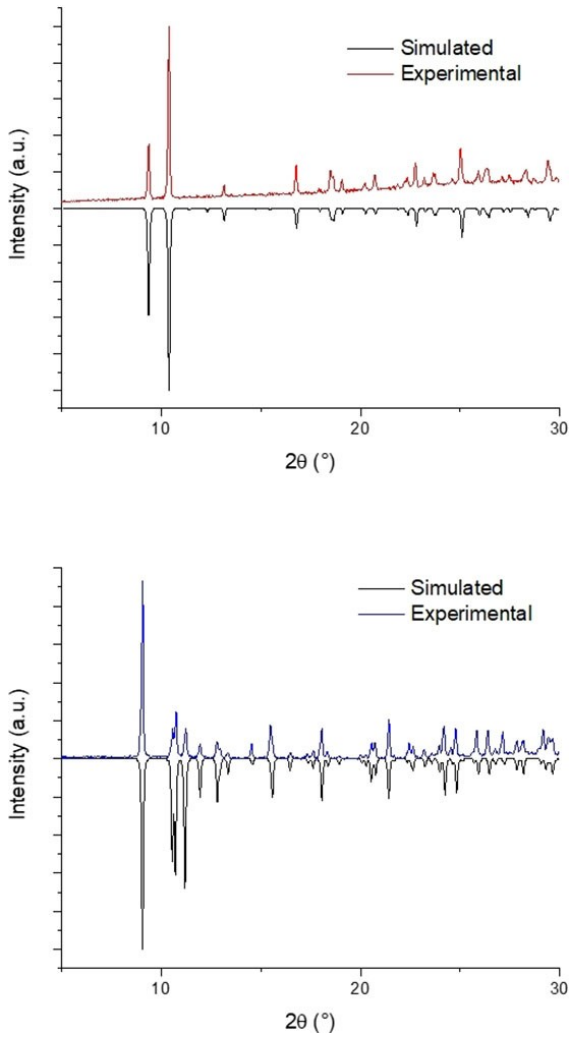

Figure 2. Top: Experimental (red) vs. theoretical (black) PXRD pattern of $[C_2mim]_n[\{Gd_2(OAc)_7\}_n]$. Bottom: Experimental (blue) vs. theoretical (black) PXRD pattern of $[C_2mim]_2[Er_2(OAc)_8]$.

a phase pure compound. However, when a 5:1 ratio was used, $[C_2mim]_n[\{Ln_2(OAc)_7\}_n]$ formed for Nd and Sm. For Pr, the 5:1 ratio already led to $Pr(OAc)_3(H_2O)$. Thus, there is a stronger tendency for the earlier lanthanides to form $Ln(OAc)_3(H_2O)$. In order to prevent its formation, a higher IL:Ln-salt ratio has to be used.

For that reason we tested a 10:1 Ln-salt ratio. Raising the amount of IL to 10 equiv. led to the dimeric compound even for Pr, Nd, and Sm, which otherwise were only obtained for the heavier lanthanides. However, close examination of the PXRD patterns revealed that only $[C_2mim]_2[Sm_2(OAc)_8]$ was phase pure, whilst for the Pr and Nd reactions, mixtures with other, yet, unidentified crystalline phases were observed.

In summary, the larger the lanthanide is, the higher the IL concentration has to be in order to lead to anhydrous complexes.

Stability and chemical reactivity

Neat products which were carefully washed with acetonitrile to remove all excess IL showed no detectable degradation over two months. However, it was noted that degradation occurred whenever excess IL was present (Figures S7 and S8). The dimeric compounds degraded faster than the polymeric ones, even in a sample container sealed under ambient atmosphere. The powder turned partially into a colorless oil, presumably due to the formation of acetic acid generated from the reaction with moisture in the air as the samples developed the characteristic smell of acetic acid.

By way of illustrative example, the polymer $[C_2mim]_n[\{Gd_2(OAc)_7\}_n]$ and the dimer $[C_2mim]_2[Er_2(OAc)_8]$ were followed using PXRD. Without washing with acetonitrile, after four weeks under ambient conditions, the PXRD pattern of the remaining powder indicated that no more dimer was present and indicated the presence of the polymeric form, as well as some undetermined crystalline compounds (Figure S7). This was later confirmed by means of a unit cell check *via* SCXRD. $[C_2mim]_n[\{Gd_2(OAc)_7\}_n]$ was also phase pure after reaction, but after four weeks degraded to $Gd(OAc)_3(H_2O)$ with other unknown phases (Figure S8). This last observation confirms that larger lanthanides seems to have a certain tendency to generate the monohydrate acetate either with a lower amount of IL or after degradation.

Structural results

The two isostructural series of anhydrous, polymeric $[C_2mim]_n[\{Ln_2(OAc)_7\}_n]$ and dimeric $[C_2mim]_2[Ln_2(OAc)_8]$ with their unit cell parameters are provided in Table 1. We next describe each series of compounds from a structural point of view.

$[C_2mim]_2[Ln_2(OAc)_8]$ (Ln = Pr, Nd, Sm, Eu, Tb–Lu), $[C_2C_2im]_2[La_2(OAc)_8]$

This family of thirteen isomorphous salts containing the discrete, dimeric $[Ln_2(OAc)_8]^{2-}$ ion all crystallized in the monoclinic space group $P2_1/n$ with one half of the dimeric anion (Figure 3) residing around a crystallographic center of inversion and one $[C_2mim]^+$ cation in the asymmetric unit. The $[C_2mim]^+$ cations are disordered with the ethyl CH_3 group being spread over three positions emulating both *cis* and *trans* conformations of a hypothetical $[C_2C_2im]^+$ cation, while the $[C_2C_2im]^+$ cation in the La structure was observed solely in the *cis*-conformation. This degree of freedom explains the isostructurality of both the $[C_2C_2im]^+$ and $[C_2mim]^+$ structures.

The Ln^{3+} cations are 9-coordinated with the oxygen atoms in the form of a slightly distorted tricapped trigonal prism. The dimeric units (Figure 3) have C_i symmetry, while each Ln coordination polyhedron is asymmetric. The Ln–Odistances range from 2.27(1) to 2.66(1) Å including minor variations with coordination mode, different data collection temperatures, and

Table 1. Comparison of cell parameters for the crystal structures determined in this study.

Compound $[C_2mim]_2[Ln_2(OAc)_8]$	*SG*	*a*, Å	*b*, Å	*c*, Å	*β*, °	*V*, Å^3	IL:Ln ratio	CCDC
$[C_2mim]_2[Pr_2(OAc)_8]$[a]	$P2_1/n$	9.535(2)	12.315(2)	16.599(3)	93.830(3)	1944.8(7)	10:1	1920417
$[C_2mim]_2[Nd_2(OAc)_8]$	$P2_1/n$	9.543(1)	12.493(1)	16.727(2)	93.596(3)	1990.4(4)	10:1	1920416
$[C_2mim]_2[Sm_2(OAc)_8]$[a]	$P2_1/n$	9.487(1)	12.260(2)	16.576(2)	93.709(5)	1924.0(5)	10:1	1920418
$[C_2mim]_2[Eu_2(OAc)_8]$[a]	$P2_1/n$	9.489(8)	12.193(2)	15.563(1)	94.220(3)	1795.8(3)	5:1	1920419
$[C_2mim]_2[Tb_2(OAc)_8]$[a]	$P2_1/n$	9.476(1)	12.132(9)	16.557(2)	94.239(9)	1898.2(3)	5:1	1920420
$[C_2mim]_2[Dy_2(OAc)_8]$[a]	$P2_1/n$	9.449(1)	12.181(1)	16.595(2)	94.155(2)	1905.1(3)	5:1	1920421
$[C_2mim]_2[Dy_2(OAc)_8]$	$P2_1/n$	9.458(5)	12.308(7)	16.690(9)	93.963(2)	1938.2(2)	5:1	1920422
$[C_2mim]_2[Ho_2(OAc)_8]$	$P2_1/n$	9.466(8)	12.300(9)	16.700(1)	93.965(3)	1939.8(3)	5:1	1920423
$[C_2mim]_2[Er_2(OAc)_8]$	$P2_1/n$	9.439(2)	12.227(3)	16.698(5)	93.968(9)	1922.5(9)	5:1	1920424
$[C_2mim]_2[Tm_2(OAc)_8]$	$P2_1/n$	9.426(2)	12.254(2)	16.685(3)	94.065(5)	1922.3(5)	5:1	1920425
$[C_2mim]_2[Yb_2(OAc)_8]$	$P2_1/n$	9.421(4)	12.255(5)	16.683(8)	94.113(2)	1921.1(2)	5:1	1920426
$[C_2mim]_2[Lu_2(OAc)_8]$	$P2_1/n$	9.408(6)	12.237(7)	16.652(9)	94.209(2)	1912.0(2)	5:1	1920427
$[C_2C_2im]_2[Ln_2(OAc)_8]$								
$[C_2C_2im]_2[La_2(OAc)_8]$[a]	$P2_1/n$	9.570(3)	12.473(4)	16.853(5)	93.685(2)	2007.4(1)	10:1	1920428
$[C_2mim]_n[\{Ln_2(OAc)_7\}_n]$								
$[C_2mim]_n[Nd_2(OAc)_7]_n$[a]	$Pca2_1$	19.240(1)	7.847(5)	19.118(1)		2886.5(3)	5:1	1920432
$[C_2mim]_n[Eu_2(OAc)_7]_n$	$Pca2_1$	19.303(3)	7.841(1)	19.138(3)		2896.5(9)	5:1	1920433
$[C_2mim]_n[Gd_2(OAc)_7]_n$	$Pca2_1$	19.281(5)	7.833(2)	19.113(5)		2886.8(9)	5:1	1920434
$[C_2mim]_n[Tb_2(OAc)_7]_n$	$Pca2_1$	19.302(1)	7.868(6)	19.113(1)		2902.7(3)	5:1	1920435

[a] Measured at 100 K.

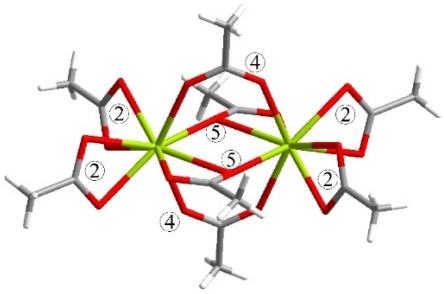

Figure 3. $[Ln_2(OAc)_8]^{2-}$ dimeric unit in the crystal structures of $[C_2mim]_2[Ln_2(OAc)_8]$ and $[C_2C_2im]_2[La_2(OAc)_8]$. Coordination modes are indicated according to Figure 1.

following the lanthanide contraction. The $[OAc]^-$ ions exhibit three coordination modes – $\eta^3\mu_2\kappa^2$, $\eta^2\mu\kappa^2$, and $\eta^2\mu_2\kappa^2$ (Figure 1).

The $\eta^2\mu_2\kappa^2$ (**4**) mode in $[C_2mim]_2[Nd_2(OAc)_8]$ represents the shortest Nd–O bond lengths in the structure – 2.41(1)–2.43(1) Å, while the $\eta^2\mu\kappa^2$ (**2**) distances are longer (2.50(1)–2.53(1) Å) as a result of partial repulsion between two O atoms binding to the same metal cation. This correlates well with the Nd–O distances observed in $[C_2mim]_2[Nd(OAc)_5]$ (2.53(1)–2.64(1) Å) represented solely by the $\eta^2\mu\kappa^2$ mode. Consequently, the $\eta^3\mu_2\kappa^2$ (**5**) mode lies in between with Nd–O = 2.437(4) and 2.541(4)–2.622(4) Å depending on how many oxygen atoms have been bound to the same metal center.

Dimeric $[Ln_2(OAc)_8]^{2-}$ units are known in the literature and even found in some applications in cryogenics,[10] but are extremely rare. The only previously published compound that contains this unit with identical coordination modes is a Gd hexaaza macrocycle complex $(2[Gd(C_{22}H_{26}N_6)\text{-}(C_2H_3O_2)_2][Gd_2(C_2H_3O_2)_8]\cdot C_6H_6\cdot 4CHCl_3)$ where $[Gd_2(OAc)_8]^{2-}$ plays the role of a counterion.[11] Hydrates such as $[Ln_2(OAc)_8(H_2O)_2]^{2-}$ have been observed with a few lanthanides (La–Sm),[12] but with different acetate coordination modes (three $\eta^2\mu\kappa^2$ and one $\eta^3\mu_2\kappa^2$ per Ln atom). Other pure, dimeric Ln tetra-carboxylato complexes include $[Eu_2(CH_3BzO)_8]^{2-}$ and $[Ho_2(\text{butenoate})_8]^{2-}$ with rather large aromatic counterions.[13] Lastly, similar tri-carboxylato dimers $[Ln_2(CH_3COO)_6(H_2O)_4]\cdot nH_2O$[10,14] have been observed for the heavier Ln (Eu–Lu) exhibiting the same $\eta^2\mu\kappa^2$ and $\eta^3\mu_2\kappa^2$ modes as the latter. Though the $\eta^2\mu_2\kappa^2$ coordination mode could still be obtained in the fluorinated $Tb_2(CF_3COO)_6(H_2O)_6$, all initial $\eta^3\mu_2\kappa^2$ bridges have been distorted resulting in $\eta^2\mu_2\kappa^2$.

$[C_2mim]_n[\{Ln_2(OAc)_7\}_n]$ (Ln = Nd, Eu-Tb)

This second isostructural series is very sensitive to the lanthanide size and the reaction ratio (5:1 IL:Ln-salt). Here the acetate ligand again shows its versatility by allowing a lower number of coordinating acetates by forming anionic polymers. These compounds crystallize in the orthorhombic space group $Pca2_1$ with two independent Ln positions and one independent cation in the asymmetric unit. The linear polymeric anion consists of repeating $[Ln_2(OAc)_7]^-$ where each Ln is coordinated by nine oxygen atoms in the form of a slightly distorted tricapped trigonal prism. Ln1 is coordinated to two chelating and five unidentate acetate ligands, while Ln2 to three chelating and three unidentate ligands. The distribution of unidentate and chelating ligands violates any possible mirror symmetry for a trigonal prism, and as a result the polymer chains are chiral with the metal ion acting as the chiral center. Both positions alternate along the *b* axis being connected by

three acetate bridges. The $[OAc]^-$ ions exhibit $\eta^3\mu_2\kappa^2$ (**5**), $\eta^2\mu\kappa^2$ (**2**), and $\eta^2\mu_2\kappa^2$ (**4**) coordination modes similar to $[C_2mim]_2[Ln_2(OAc)_8]$; however, the proportion of the terminating $\eta^2\mu\kappa^2$ mode is significantly lower (Figure 4).

To analyze the bonding patterns we will use $[C_2mim]_n[\{Nd_2(OAc)_7\}_n]$ as an example. In addition to two symmetry-independent Nd positions, there are seven independent acetate ions resulting in a wide spread of the Nd–O bonds (2.36(1)–2.77(1) Å). Although the Nd–O bonds in different coordination modes show partial overlap, the monodentate coordinated $[OAc]^-$ ($\eta^2\mu_2\kappa^2$ and in part $\eta^3\mu_2\kappa^2$ similarly to $[C_2mim]_2[Nd_2(OAc)_8]$) cover the lower range of that spectrum – 2.365(7)–2.497(6) Å, while the bidentate $[OAc]^-$ ($\eta^2\mu\kappa^2$ and $\eta^3\mu_2\kappa^2$) partially overlapping the upper one, 2.446(7)–2.767(6) Å. These distances are also comparable to those in the two known Nd acetates[15] (see below).

Among the published Nd acetates, $[C_2mim]_n[\{Nd_2(OAc)_7\}_n]$ is structurally closer to the acetate hemihydrate $Nd(OAc)_3\cdot 0.5\,H_2O$[15a] or the Pr acetate monohydrate[16] than to the anhydrous $Nd(OAc)_3$.[15b] The two former exhibits a linear polymeric chain with similar acetate coordination modes – only $\eta^3\mu_2\kappa^2$ and $\eta^2\mu_2\kappa^2$. Both crystallographically independent Ln positions in $Nd(OAc)_3\cdot 0.5\,H_2O$ and $Pr(OAc)_3\cdot H_2O$ are nine-coordinated in the form of distorted tricapped trigonal prisms. $Nd(OAc)_3$ crystallizes with ten independent Nd positions and in addition to $\eta^3\mu_2\kappa^2$ introduces two new coordination modes – $\eta^3\mu_3\kappa^2$ (**6**) and $\eta^4\mu_3\kappa^2$ (**7**). The Nd positions are mostly 9-coordinated with coordination polyhedra that are significantly more irregular capped trigonal prisms. Polymeric chains are also present in the structure, but due to additional $Nd(OAc)_n$ groups, with the new coordination modes $\eta^3\mu_3\kappa^2$ and $\eta^4\mu_3\kappa^2$, they merge into layers.

Among the related polymeric Ln acetates an even more complex connectivity has been observed in catena-(μ^4-acetato)-(μ^3-acetato)-bis(μ^2-acetato)-aqua-di-europium(II)[17] introducing another coordination mode $\eta^5\mu_4\kappa^2$ (**8**) resulting in a denser layered motif. It is also worth noting that the acetate anion may offer plenty of other coordination modes, for example, $\eta^4\mu_4\kappa^2$, $\eta^5\mu_5\kappa^2$ or $\eta^6\mu_5\kappa^2$, though they have so far not been observed in pure lanthanide compounds.

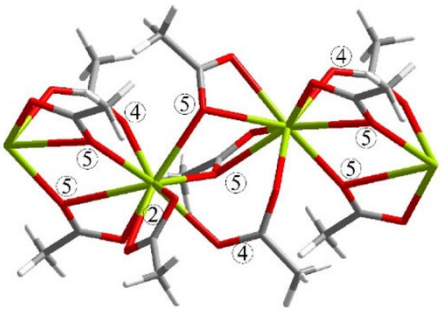

Figure 4. Polymeric chain $[\{Nd_2(OAc)_7\}_n]^-$ in the crystal structure of $[C_2mim]_n[\{Nd_2(OAc)_7\}_n]$. Coordination modes are indicated according to Figure 1.

Vibrational spectroscopy

The different coordination modes also show in the infrared spectra of the compounds. $[C_2mim]_2[Er_2(OAc)_8]$, and $[C_2mim]_n[\{Gd_2(OAc)_7\}_n]$, were chosen as representatives for each of the two structure series.

Acetates have been intensively studied by vibrational spectroscopy since the 1950s.[18] Conveniently, sodium acetate was used as a standard for the comparison of acetates. It is known to show two significant peaks at 1440 (CH_3 deformation) and 1578 (C–O stretching) cm^{-1}.[19] IR data for the IL $[C_2mim][OAc]$ shows the values of the two peaks of the anion be shifted to 1377 (CH_3 deformation) and 1560 (C–O stretching) cm^{-1} (Figure S13).

IR spectra of the dimeric and polymeric compounds reveal the non-equivalency of the acetate oxygen atoms. In the dimeric $[C_2mim]_2[Er_2(OAc)_8]$, there are now three peaks for the acetate at 1404 (CH_3 deformation), 1566 (C–O stretching) and 1608 (C–O stretching) cm^{-1} (Figure S16). The deformation of the methyl group seems to be similar whatever the type of coordination is. However, there are two types of carbon-oxygen stretching signals, which confirm the presence of, at least, two different types of coordination modes in the compound.[20] It could be also related to the crystal structure bond lengths. The ligands only coordinated to one metal center have bond lengths (C–O) around 2.41 Å whereas when the acetate ligand bridged the two metal centers the bond lengths are between 2.31–2.57 Å.

In the polymeric $[C_2mim]_n[\{Gd_2(OAc)_7\}_n]$, there are four bands at 1405 (CH_3 deformation), 1433 (CH_3 deformation), 1566 (C–O stretching), and 1605 (C–O stretching) cm^{-1} (Figure S15). It seems that in this case the methyl group vibrational frequency is impacted by the type of coordination because of the hydrogen bonding between some CH_3 groups and the oxygen from the bridged acetates. Nevertheless, in the polymeric compounds the C–O bonds lengths are very similar (2.30–2.42 Å) except one (2.86 Å) from the $\eta^3\mu_2\kappa^2$ coordination mode.

In summary, IR can be used to distinguish between the two different complexes *via* the stretching signals of the C–O and CH_3 functions. The differences between the bands can be correlated to the bond lengths and coordination modes as observed from the SCXRD analyses.

Thermal properties

To elucidate the thermal properties of the two structure series, differential scanning thermograms of the two representatives for the two series, $[C_2mim]_2[Er_2(OAc)_8]$, and $[C_2mim]_n[\{Gd_2(OAc)_7\}_n]$, were recorded. Upon heating $[C_2mim]_n[\{Gd_2(OAc)_7\}_n]$ (Figure 5, top) two clear endothermic phase transitions close to each other can be observed. The first transition starts at 180.2 °C, followed by a second at 188.5 °C. Polarized optical microscopy (POM) indicated a transition of the crystalline solid to a higher order mesophase (Figure S17) before melting into an isotropic liquid.

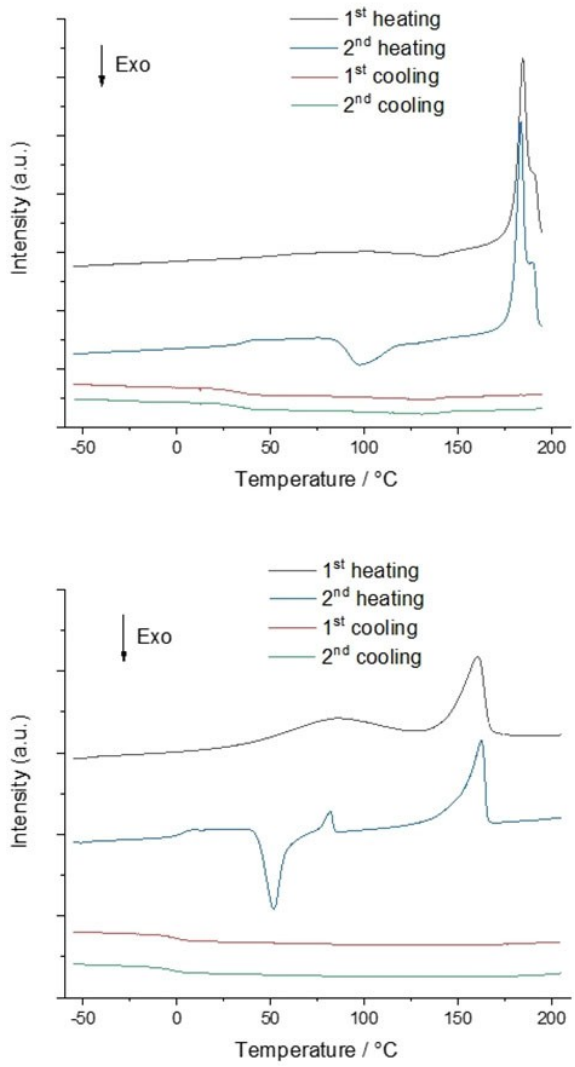

Figure 5. DSC thermograms of top: $[C_2mim]_n[Gd_2(OAc)_7]_n$ and bottom: $[C_2mim]_2[Er_2(OAc)_8]$.

During the cooling, vitrification can be observed around 33 °C. This reversible process occurs around 35 °C during the second heating. The compound recrystallized upon heating at 86.5 °C (a small feature of this recrystallization process can be even detected in the first heating cycle) and yielded to the mesophase at 179.4 °C, becoming an isotropic liquid at 187.8 °C. Noteworthy, the second heating shows a slightly better separation between the phase transitions from solid to liquid. Indicating that repeated heating and cooling cycle help to enhance crystallinity. All subsequent heating and cooling cycles are fully reproducible.

The reversible cold crystallization and melting of coordination polymers upon heating is well known among halometallate[21] and other organometallic ILs.[5h,22] The metal coordination environment and complex formation in such systems can vary under different conditions of temperature and pressure even when the composition is held constant.[23] Anhydrous imidazolium salts of $[Ln(OAc)_5]^{2-}$ ions had not been reported to crystallize under the conditions explored here.[3] The unpredictable nature of polymeric metal containing ILs along with the highly flexible coordination chemistry of the chosen anion ($[OAc]^-$) along with some unreported experimental data strongly imply the existence of yet more undiscovered complexes in the $[C_nmim][OAc]/Ln^{3+}$ systems, which we hope to continue to explore.

The DSC trace of the first heating of the dimeric compound $[C_2mim]_2[Er_2(OAc)_8]$ (Figure 5, bottom) shows a broad endothermic event between 60 to 130 °C which is attributed to the loss of residual acetonitrile. A broad signal at 146.4 °C indicated a melting from solid to isotropic liquid. Upon cooling a vitrification can be observed around 0 °C. The devitrification occurred around 3.5 °C during subsequent heating. A cold recrystallization was observed at 43.4 °C followed by a solid-solid phase transition at 76.6 °C. This seems to indicate that the compound could have another structural conformation. However it has not been possible to determine it. The compound started to melt at 153.4 °C again with the event extending over several degrees. The second cooling was similar to the previous one with again only one vitrification around 0 °C, and the subsequent third heating cycle was similar to the second.

The dimer melts about 50 °C before the polymer. This can be attributed on the one hand to the lower degree of condensation, that is, less polymeric character of the dimer, but also to reduced connectivity. This might also be the reason, why the polymeric compound features a mesophase, while the coordination dimer displays only a second crystalline phase.

Conclusion

In summary, we have developed a straightforward synthetic route, based on ionic liquids, towards two anhydrous lanthanide acetate series from their corresponding metal salt hydrates, polymeric $[C_2mim]_n[\{Ln_2(OAc)_7\}_n]$ and dimeric $[C_2mim]_2[Ln_2(OAc)_8]$. PXRD data indicated that for IL:Ln-salt ratios of 5:1, for the heavier lanthanides, that is, Ln = Dy–Lu, the formation of $[C_2mim]_2[Ln_2(OAc)_8]$ is preferred, whilst for the lighter lanthanides, Ln = Nd, Sm, Gd, polymeric $[C_2mim]_n[\{Ln_2(OAc)_7\}_n]$ is found. The structural preference crosses over at Ln = Eu and Tb, for which both structures are found. Under the same conditions for La and Pr, only $Ln(OAc)_3(H_2O)$ was isolated. From this one could conclude, that the larger the lanthanide ion is, the higher the tendency to form the lanthanide acetate hydrate. When reducing the IL:Ln-salt ratio to 3:1, even for Ln = Pr, Nd, and Sm, $Ln(OAc)_3(H_2O)$ forms. When a higher IL:Ln-salt ratio of 10:1 is employed, even for Ln = Pr, Nd and Sm, the formation of the dimeric structure is observed. Thus, it appears that a large (e.g., tenfold) excess of IL the formation of the dimer $[C_2mim]_2[Ln_2(OAc)_8]$ is favored for all lanthanides, regardless of their size. This appears to be plausible, as the IL:Ln-salt ratio is higher in $[C_2mim]_2[Ln_2(OAc)_8]$ (which corresponds to 1:1 of $[C_2mim][OAc]\cdot Ln(OAc)_3$) than in $[C_2mim]_n[\{Ln_2(OAc)_7\}_n]$ (which just has a 1:2 ratio according to its composition $0.5\,[C_2mim][OAc]\cdot Ln(OAc)_3$). For La, the use of an IL with a

bulkier cation, that is, $[C_2C_2im]_2[OAc]$, allowed access the dimer $[C_2C_2im]_2[La_2(OAc)_8]$, even from aqueous solution.

Both the dimeric and polymeric structures reveal the same acetate coordination modes, namely $\eta^3\mu_2\kappa^2$, $\eta^2\mu\kappa^2$, and $\eta^2\mu_2\kappa^2$, though with slightly different proportion. The dimeric complexes show low lanthanide size selectivity, though the largest in the series, La, could be crystallized isostructurally only with a larger cation. On the other hand, the acetate anion has been found to be very "creative," offering extended variety of connectivities with the lanthanide cations and, as a result, multiple formations with the same metal enhancing our interest for further investigations. The formation of the different complexes with their different coordination modes can be easily identified through IR spectroscopy according to the different stretching modes of the C–O and CH_3 groups. The thermal properties of both compound series can be related well to their structural features. As expected, due to the higher degree of condensation, that is, connectivity, the compounds with polymeric structure melt at higher temperatures (ca. 50 °C) than the dimeric ones. For both compounds, before melting the formation of another form is observed. In case of the dimeric material, this is a second solid crystalline phase, whilst in case of the polymeric structure polarizing optical microscopy reveals the formation of a mesophase.

The straightforward methodology established in this work has allowed the formation of extremely rare dimeric $[Ln_2(OAc)_8]^{2-}$ units with a large number of lanthanides which could lead to potential applications depending on the Ln used (magnetism, optical properties, etc.). Moreover some reactions generated either undiscovered phases from the thermal behavior or some undetermined compounds as minority phases observed in PXRD. Taking into account the simplicity of the ligand combined with a huge variety of coordination modes it can deliver, the IL/Ln-acetate systems still lack deeper understanding and represent a considerable interest in terms of designed synthesis of specific anhydrous lanthanide complexes. There is obviously much room left to explore.

Experimental Section

Syntheses: 1-Methylimidazole (98%, Alfa Aesar, Karlsruhe, Germany) and 1-ethylimidazole (>98%, Tokyo Chemical Industry, Tokyo, Japan) were distilled over KOH before use. Lanthanide chloride hydrates were obtained from the reaction between Ln_2O_3 (HEFA Rare Earth Canada Co. Ltd, Richmond, BC, Canada) and HCl (37%, VWR Chemicals, Fontenay-sous-Bois, France). Ethyl bromide (98%, Alfa Aesar, Karlsruhe, Germany) and sodium acetate (99%, Alfa Aesar) were used as received. All solvents were 'solvent grade' and used as received without additional purification.

Synthesis of $[C_2C_nim][Br]$: In a flask under argon were introduced 1-alkylimidazole (50 mmol, 1.0 equiv.), ethyl bromide (55 mmol, 1.1 equiv.) and acetonitrile (5 mL). The mixture was heated under reflux for three days. After cooling to room temperature the solution was washed with ethyl acetate and put in a cold bath (−78 °C) to allow the crystallization of the product. The white precipitate was washed several times and then dried under vacuum at room temperature.

$[C_2mim][Br]$ FTIR (υ (cm^{-1})): 3422, 3136, 3065, 3027, 2975, 2866, 2822, 1770, 1731, 1670, 1571, 1519, 1467, 1446, 1423, 1386, 1366, 1340, 1302, 1251, 1171, 1110, 1093, 1032, 957, 909, 865, 789, 704, 665, 649, 621, 599, 418.

$[C_2C_2im][Br]$ FTIR (υ (cm^{-1})): 3129, 3056, 2976, 2938, 2796, 2730, 2608, 1563, 1544, 1447, 1408, 1384, 1347, 1295, 1247, 1165, 1122, 1087, 1028, 956, 821, 802, 755, 688, 625, 592.

Synthesis of $[C_2C_nim][OAc]$: $[C_2C_nim][Br]$ (50 mmol, 1.0 equiv.) and sodium acetate (4.10 g, 50 mmol, 1.0 equiv.) were dissolved in acetone (50 mL) in a round bottom flask. The mixture was stirred overnight then filtrated. The filtrate was evaporated under reduced pressure to yield to a colorless oil.

$[C_2mim][OAc]$ FTIR (υ (cm^{-1})): 3139, 2975, 3030, 2866, 2748, 1560, 1451, 1427, 1377, 1328, 1256, 1174, 1090, 1002, 1034, 958, 899, 804, 702, 599, 454.

$[C_2C_2im][OAc]$ FTIR (υ (cm^{-1})): 3422, 3136, 3064, 2978, 2933, 1562, 1410, 1165, 1123, 1090, 1045, 1009, 956, 921, 830, 802, 760, 688, 642, 622, 527, 461.

General procedure for the synthesis of anhydrous lanthanide compounds: In a round-bottom flask were introduced $LnCl_3 \cdot xH_2O$ ($x = 6$ or 7; 1.0 mmol, 1.0 equiv.) and $[C_2mim][OAc]$ (850 mg, 5.0 mmol, 5.0 equiv.). The mixture was heated at 100 °C under stirring overnight. The flask was then transferred to a pre-heated oven at 100 °C. A program was run to slowly decrease the temperature (1 °C h^{-1}) to 25 °C to allow a better crystallization of the final products. The final complexes have been obtained with yields 80% and higher.

$La(OAc)_3(H_2O)$. White solid. FTIR (υ (cm^{-1})): 3262, 1601, 1523, 1402, 1335, 1052, 1015, 942, 663, 614, 465, 419.

$Pr(OAc)_3(H_2O)$. Light green solid. FTIR (υ (cm^{-1})): 3273, 1682, 1531, 1395, 1341, 1170, 1052, 1024, 1007, 956, 943, 748, 670, 642, 610, 502, 477, 421.

$[C_2mim]_n[\{Nd_2(OAc)_7\}_n]$. White solid. FTIR (υ ($cm^{-1}$)): 3148, 3119, 3090, 3079, 2987, 2929, 1634, 1569, 1391, 1335, 1254, 1167, 1121, 1090, 1048, 1015, 940, 867, 808, 774, 646, 620, 500. ESI TOF *m/z* (negative mode) 700.4110 (calcd *m/z* 700.9145).

$[C_2mim]_n[\{Sm_2(OAc)_7\}_n]$. White solid. FTIR (υ ($cm^{-1}$)): 3142, 3117, 3098, 3079, 2975, 2931, 1609, 1554, 1402, 1336, 1247, 1166, 1118, 1086, 1047, 1013, 942, 869, 808, 775, 641, 666, 611, 489. ESI TOF *m/z* (negative mode) 718.6951 (calcd *m/z* 718.9356).

$[C_2mim]_n[\{Eu_2(OAc)_7\}_n]$ and $[C_2mim]_2[Eu_2(OAc)_8]$ (mixture). White solid. FTIR (υ (cm^{-1})): 3380, 3143, 3093, 2999, 2984, 2943, 1605, 1565, 1432, 1404, 1335, 1300, 1249, 1160, 1095, 1045, 1015, 953, 932, 868, 787, 680, 666, 642, 626, 613, 504, 469. $[C_2mim]_n[\{Eu_2(OAc)_7\}_n]$ ESI TOF *m/z* (negative mode) 716.6241 (calcd *m/z* 716.9348). $[C_2mim]_2[Eu_2(OAc)_8]$ ESI TOF *m/z* (negative mode) 387.6951 (calcd *m/z* 387.9743).

$[C_2mim]_n[\{Gd_2(OAc)_7\}_n]$. White solid. FTIR (υ ($cm^{-1}$)): 3143, 3093, 2984, 1606, 1566, 1434, 1405, 1336, 1300, 1161, 1095, 1045, 1016, 954, 933, 868, 787, 667, 651, 643, 626, 613, 505, 469. ESI TOF *m/z* (negative mode) 730.6341 (calcd *m/z* 730.9448).

$[C_2mim]_n[\{Tb_2(OAc)_7\}_n]$ and $[C_2mim]_2[Tb_2(OAc)_8]$ (mixture). Brown solid. FTIR (υ (cm^{-1})): 3550, 3526, 3360, 3150, 3109, 2994, 2932, 1643, 1590, 1543, 1407, 1351, 1338, 1162, 1099, 1054, 1018, 949, 939, 861, 787, 742, 691, 668, 643, 615, 506, 484, 468, 453, 425. $[C_2mim]_n[\{Tb_2(OAc)_7\}_n]$ ESI TOF *m/z* (negative mode) 730.6166 (calcd *m/z* 730.9444). $[C_2mim]_2[Tb_2(OAc)_8]$ ESI TOF *m/z* (negative mode) 394.6952 (calcd *m/z* 394.9791).

$[C_2mim]_2[Dy_2(OAc)_8]$. White solid. FTIR (υ (cm^{-1})): 3546, 3372, 3238, 3150, 3109, 3002, 2933, 1592, 1544, 1408, 1351, 1162, 1099, 1053, 1018, 950, 940, 900, 861, 788, 692, 669, 644, 616, 508, 470, 441, 428, 417. ESI TOF *m/z* (negative mode) 398.6946 (calcd *m/z* 398.9817).

$[C_2mim]_2[Ho_2(OAc)_8]$. Light pink solid. FTIR (υ (cm^{-1})): 3142, 3092, 3002, 2985, 2945, 1609, 1568, 1435, 1406, 1347, 1335, 1301, 1248, 1161, 1095, 1045, 1015, 957, 934, 871, 808, 788, 751, 682, 668, 644, 607, 508, 466. ESI TOF *m/z* (negative mode) 400.7019 (calcd *m/z* 400.9841).

$[C_2mim]_2[Er_2(OAc)_8]$. Light pink solid. FTIR (υ (cm^{-1})): 3385, 3143, 3092, 2985, 1608, 1566, 1404, 1335, 1301, 1249, 1161, 1094, 1045, 1016, 958, 934, 871, 789, 682, 668, 645, 614, 509, 469, 426. ESI TOF *m/z* (negative mode) 402.6986 (calcd *m/z* 402.9851).

$[C_2mim]_2[Tm_2(OAc)_8]$. White solid. FTIR (υ (cm^{-1})): 3396, 3154, 3118, 2993, 1560, 1400, 1347, 1169, 1048, 1016, 981, 963, 945, 905, 867, 845, 670, 652, 617, 516, 496, 471. ESI TOF *m/z* (negative mode) 404.6964 (calcd *m/z* 404.9880).

$[C_2mim]_2[Yb_2(OAc)_8]$. White solid. FTIR (υ (cm^{-1})): 3388, 3153, 3090, 2995, 1618, 1570, 1404, 1345, 1299, 1249, 1169, 1097, 1047, 1018, 959, 930, 878, 793, 687, 671, 643, 618, 512, 474, 425. ESI TOF *m/z* (negative mode) 409.0997 (calcd *m/z* 409.4923).

$[C_2mim]_2[Lu_2(OAc)_8]$. White solid. FTIR (υ (cm^{-1})): 3384, 1638, 1540, 1453, 1412, 1169, 1049, 1022, 957, 839, 759, 688, 642, 613, 509. ESI TOF *m/z* (negative mode) 410.6987 (calcd *m/z* 410.9945).

Compounds obtained with a 3:1 (IL/Ln-ratio): $Nd(OAc)_3(H_2O)$. Light purple solid. FTIR (υ (cm^{-1})): 3276, 1682, 1598, 1528, 1395, 1341, 1052, 1024, 1006, 956, 942, 863, 744, 670, 642, 609, 571, 504, 477.

$Sm(OAc)_3(H_2O)$. White solid. FTIR (υ (cm^{-1})): 3336, 1705, 1531, 1415, 1263, 1051, 1018, 951, 674, 643, 612, 501, 464.

Compounds obtained with a 10:1 (IL/Ln-ratio): $[C_2mim]_2[Pr_2(OAc)_8]$. Light green solid. ESI TOF *m/z* (negative mode) 376.6848 (calcd *m/z* 376.9609).

$[C_2mim]_2[Nd_2(OAc)_8]$. Light purple solid. ESI TOF *m/z* (negative mode) 378.6852 (calcd *m/z* 378.9627).

$[C_2mim]_2[Sm_2(OAc)_8]$. White solid. FTIR (υ (cm^{-1})): 3144, 3094, 2999, 2984, 2931, 1602, 1564, 1430, 1404, 1336, 1300, 1249, 1160, 1095, 1045, 1015, 951, 930, 866, 786, 679, 665, 641, 626, 613, 502, 469, 429. ESI TOF *m/z* (negative mode) 388.6932 (calcd *m/z* 388.9747).

General procedure for the synthesis of $[C_2C_2im][La_2(OAc)_8]$: In a round-bottom flask were introduced $LaCl_3 \cdot 7H_2O$ (371 mg, 1.0 mmol, 1 equiv.), $[C_2C_2im][OAc]$ (1.840 g, 10 mmol, 10 equiv.), and water (5 mL). The mixture was heated at 100 °C under stirring overnight. The flask was then transferred to a pre-heated oven at 100 °C. A program was run to slowly decrease the temperature (1 °C h^{-1}) to allow a better crystallization of the final product.

Instrumentation: PXRD data were recorded at ambient temperature on a PANalytical X'pert PRO diffractometer (Malvern Panalytical, Malvern, UK), operating at 45 kV and 40 mA and using $Cu_{K\alpha1}$ radiation. The data were recorded in reflection mode from 5° to 70° with a step size of 0.01° for 60 min.

The data for single crystal analysis at Stockholm University were collected on a Bruker Venture diffractometer (Bruker AXS, Karlsruhe, Germany) using $Cu_{K\alpha}$ radiation ($\lambda = 1.54178$ Å at 297 K) at room temperature or at low temperature (100 K). The crystal structures were solved and refined using SHELXT and SHELXL subroutines within the APEX3 software package.[24] Absorption corrections were carried out with the program SADABS. Hydrogen atoms for all structures were assigned geometrically using a riding atom model. To illustrate the crystal structures, the program Diamond 3 (CrystalImpact, Bonn, Germany) was used.[25]

The crystal structural measurements at The University of Alabama were carried out on a Bruker SMART APEX II CCD diffractometer ($Mo_{K\alpha}$ radiation; $\lambda = 0.71073$ Å) at 100 K. The intensity data of the reflections and scaling were integrated using SAINT within the APEX3 software package.[26] SADABS[27] was used for the absorption corrections. The crystal structure solution was performed by direct methods using SHELXT.[28] SHELXL-97[26] and SHELXL-2013[24c] were used for subsequent difference Fourier analyses and least-squares refinement. All non-hydrogen atoms were refined anisotropically, whereas hydrogen atoms were assigned geometrically using a riding atom model.

Differential scanning calorimetry (DSC) was performed with a computer-controlled PhoenixDSC 204 F1 thermal analyzer (Netzsch, Selb, Germany). Measurements were carried out at a heating rate of 5 °C min^{-1} from −60 to 210 °C in sealed aluminum crucible with a nitrogen flow rate of 40 mL min^{-1}. The samples were placed in aluminum pans which were cold-sealed and punctured. Before recording the DSC thermogram the samples were cooled to −60 °C. Given temperatures correspond to the onset.

A SYNAPT G2-S HDMS Q-ToF Mass Spectrometer (Waters, Manchester, United Kingdom) with an electrospray ionization (ESI) operated in the positive and negative ion mode, was used in this study. The ion source was set up as follows: capillary voltage: 2500 V, extractor: 1.0 V, RF lens: 0.5 V, ion source temperature: 120 °C and desolvation temperature 250 °C. Nitrogen was used as both the cone and desolvation gas at a flow of 70 L h^{-1} and 500 L h^{-1}, respectively. Argon was used as a collision gas at a pressure of $2.95 \cdot 10^{-4}$ mbar.

The infrared spectroscopy (IR) was conducted with a Bruker Alpha-P ATR-spectrometer (Bruker AXS) in attenuated total reflection configuration in the range of 4000–400 cm^{-1}. The data evaluation was carried out with the program OPUS (Bruker, Ettlingen, Germany).

Optical analyses were made by heated-stage polarized optical microscopy (POM) with an Axio Imager A1 microscope (Carl Zeiss Micro Imaging GmbH, Göttingen, Germany) equipped with a hot stage, THMS600 (Linkam Scientific Instruments Ltd, Surrey, UK), and Linkam TMS 94 temperature controller (Linkam Scientific Instruments Ltd). Images were recorded at a magnification of 100× as a video with a digital camera. During heating and cooling, the sample was placed between two cover slips. Heating and cooling rates were 10 °C min^{-1}.

Deposition numbers 1920416, 1920417, 1920418, 1920419, 1920420, 1920421, 1920422, 1920423, 1920424, 1920425, 1920426, 1920427, 1920428, 1920432, 1920433, 1920434, and 1920435 contain the supplementary crystallographic data for this paper. These data are provided free of charge by the joint Cambridge Crystallographic Data Centre and Fachinformationszentrum Karlsruhe Access Structures service www.ccdc.cam.ac.uk/structures.

Acknowledgements

This research was supported, in part, by the Royal Swedish Academy of Science through the Göran Gustafsson prize to A.-V.M., by the Swedish Research Council (Vetenskapsrådet, VR) through Grant 2020-05405 (A.-V.M.), by a Tage Erlander Guest Professorship to R.D.R. (VR Grant 2018-00233), and by U.S. Department of Energy, Office of Science, Office of Basic Energy

Sciences, Heavy Elements program under Award DE-SC0019220 (to R.D.R.). S.-F.T. acknowledges financial support from the Qingdao Science and Technology Program (19-6-1-43 nsh).

Conflict of Interest

The authors declare no conflict of interest.

Keywords: anhydrous lanthanide complexes · dimers · ethylmethylimidazolium acetate · polymers

[1] a) S. Bette, J. Stelzner, G. Eggert, T. Schleid, G. Matveeva, U. Kolb, R. E. Dinnebier, *Angew. Chem. Int. Ed.* **2020**, *59*, 9438–9442; *Angew. Chem.* **2020**, *132*, 9525–9529; b) U. Kumar, J. Thomas, N. Thirupathi, *Inorg. Chem.* **2010**, *49*, 62–72.
[2] V. Smetana, S. P. Kelley, H. M. Titi, X. Hou, S.-F. Tang, A.-V. Mudring, R. D. Rogers, *Inorg. Chem.* **2020**, *59*, 818–828.
[3] a) G. G. Sadikov, G. A. Kukina, M. A. Porai-Koshits, L. A. Pospelova, *J. Struct. Chem.* **1968**, *9*, 128–129; b) G. Meyer, D. Gieseke-Vollmer, *Z. Anorg. Allg. Chem.* **1993**, *619*, 1603–1608; c) C. J. Kepert, L. Wei-Min, P. C. Junk, B. W. Skelton, A. H. White, *Aust. J. Chem.* **1999**, *52*, 437–458.
[4] a) S. P. Kelley, V. Smetana, S. D. Emerson, A.-V. Mudring, R. D. Rogers, *Chem. Commun.* **2020**, *56*, 4232–4235; b) S.-F. Tang, V. Smetana, M. K. Mishra, S. P. Kelley, O. Renier, R. D. Rogers, A.-V. Mudring, *Inorg. Chem.* **2020**, *59*, 7227–7237; c) D. Yaprak, E. T. Spielberg, T. Bäcker, M. Richter, B. Mallick, A. Klein, A.-V. Mudring, *Chem. Eur. J.* **2014**, *20*, 4704–4712.
[5] a) D. Prodius, A.-V. Mudring, in *Handbook on the Physics and Chemistry of Rare Earths, Vol. 50* (Eds.: J.-C. G. Bünzli, V. K. Pecharsky), Elsevier, **2016**, pp. 395–420; b) A. Babai, A.-V. Mudring, *Chem. Mater.* **2005**, *17*, 6230–6238; c) A. Babai, S. Pitula, A. V. Mudring, *Eur. J. Inorg. Chem.* **2010**, *2010*, 4933–4937; d) A. Babai, A.-V. Mudring, *Inorg. Chem.* **2006**, *45*, 3249–3255; e) A. Babai, A.-V. Mudring, *Dalton Trans.* **2006**, 1828–1830; f) S.-F. Tang, A.-V. Mudring, *Cryst. Growth Des.* **2009**, *9*, 2549–2551; g) S. Tang, A.-V. Mudring, *Cryst. Growth Des.* **2011**, *11*, 1437–1440; h) E. T. Spielberg, E. Edengeiser, B. Mallick, M. Havenith, A.-V. Mudring, *Chem. Eur. J.* **2014**, *20*, 5338–5345.
[6] a) B. Mallick, B. Balke, C. Felser, A. V. Mudring, *Angew. Chem. Int. Ed.* **2008**, *47*, 7635–7638; *Angew. Chem.* **2008**, *120*, 7747–7750; b) A. Getsis, A. V. Mudring, *Z. Anorg. Allg. Chem.* **2010**, *636*, 1726–1734; c) S. Tang, A. Babai, A.-V. Mudring, *Angew. Chem. Int. Ed.* **2008**, *47*, 7631–7634; *Angew. Chem.* **2008**, *120*, 7743–7746; d) B. Mallick, B. Balke, C. Felser, A.-V. Mudring, *Angew. Chem. Int. Ed.* **2008**, *47*, 7635–7638; *Angew. Chem.* **2008**, *120*, 7747–7750.
[7] a) A. S. Chesman, M. Yang, N. D. Spiccia, G. B. Deacon, S. R. Batten, A. V. Mudring, *Chem. Eur. J.* **2012**, *18*, 9580–9589; b) A. S. Chesman, M. Yang, B. Mallick, T. M. Ross, I. A. Gass, G. B. Deacon, S. R. Batten, A.-V. Mudring, *Chem. Commun.* **2012**, *48*, 124–126.
[8] C. C. Hines, D. B. Cordes, S. T. Griffin, S. I. Watts, V. A. Cocalia, R. D. Rogers, *New J. Chem.* **2008**, *32*, 872–877.
[9] S. Cotton, *Lanthanide and Actinide Chemistry*, Wiley, Chichester, **2013**.
[10] a) G. Lorusso, O. Roubeau, M. Evangelisti, *Angew. Chem. Int. Ed.* **2016**, *55*, 3360–3363; *Angew. Chem.* **2016**, *128*, 3421–3424; b) M. Evangelisti, O. Roubeau, E. Palacios, A. Camón, T. N. Hooper, E. K. Brechin, J. J. Alonso, *Angew. Chem. Int. Ed.* **2011**, *50*, 6606–6609; *Angew. Chem.* **2011**, *123*, 6736–6739.
[11] P. H. Smith, R. R. Ryan, *Acta Crystallogr. Sect. C* **1992**, *48*, 2127–2130.
[12] H. Sawase, Y. Koizumi, Y. Suzuki, M. Shimoi, A. Ouchi, *Bull. Chem. Soc. Jpn.* **1984**, *57*, 2730–2737.
[13] a) B. V. Bukvetskii, I. V. Kalinovskaya, *Russ. J. Inorg. Chem.* **2011**, *56*, 721–725; b) A. M. Atria, M. T. Garland, R. Baggio, *Acta Crystallogr. Sect. C* **2012**, *68*, m185-m188.
[14] a) R. Vaďura, J. Kvapil, *Mater. Res. Bull.* **1971**, *6*, 865–873; b) B. Barja, R. Baggio, M. T. Garland, P. F. Aramendia, O. Peña, M. Perec, *Inorg. Chim. Acta* **2003**, *346*, 187–196; c) J. W. Bats, R. Kalus, H. Fuess, *Acta Crystallogr. Sect. B* **1979**, *35*, 1225–1227; d) C. J. Kepert, L. Wei-Min, P. C. Junk, B. W. Skelton, A. H. White, *Aust. J. Chem.* **1999**, *52*, 437–458; e) L. Cañadillas-Delgado, O. Fabelo, J. Cano, J. Pasán, F. S. Delgado, F. Lloret, M. Julve, C. Ruiz-Pérez, *CrystEngComm* **2009**, *11*, 2131–2142.
[15] a) S. Gomez Torres, *Thesis*, Köln, Germany, **2007**; b) S. Gomez Torres, G. Meyer, *Z. Anorg. Allg. Chem.* **2008**, *634*, 231–233.
[16] S. Ganapathy, V. P. Chacko, R. G. Bryant, M. C. Etter, *J. Am. Chem. Soc.* **1986**, *108*, 3159–3165.
[17] P. Starynowicz, *J. Alloys Compd.* **1998**, *268*, 47–49.
[18] K. Ito, H. J. Bernstein, *Can. J. Chem.* **1956**, *34*, 170–178.
[19] L. H. Jones, E. McLaren, *J. Chem. Phys.* **1954**, *22*, 1796–1800.
[20] D. G. Karraker, *J. Inorg. Nucl. Chem.* **1969**, *31*, 2815–2832.
[21] B. Mallick, A. Metlen, M. Nieuwenhuyzen, R. D. Rogers, A.-V. Mudring, *Inorg. Chem.* **2012**, *51*, 193–200.
[22] A.-V. Mudring, *Aust. J. Chem.* **2010**, *63*, 544–564.
[23] J. Estager, J. D. Holbrey, M. Swadzba-Kwasny, *Chem. Soc. Rev.* **2014**, *43*, 847–886.
[24] a) Bruker, **2015**; b) G. M. Sheldrick, *Acta Crystallogr. Sect. A* **2015**, *71*, 3–8; c) G. M. Sheldrick, *Acta Crystallogr. Sect. C* **2015**, *71*, 3–8.
[25] K. Brandenburg, H. Putz, *Crystal Impact GbR*, Bonn, Germany, **2011**.
[26] G. Sheldrick, *Acta Crystallogr. Sect. A* **2008**, *64*, 112–122.
[27] L. Krause, R. Herbst-Irmer, D. Stalke, *J. Appl. Crystallogr.* **2015**, *48*, 1907–1913.
[28] G. M. Sheldrick, *Acta Crystallogr. Sect. A* **2015**, *71*, 3–8.

Manuscript received: January 13, 2021
Accepted manuscript online: June 7, 2021
Version of record online: August 12, 2021

